

Neutron bursts associated with thunderstorms

A. Chilingarian,* N. Bostanjyan, and L. Vanyan

A. Alikhanyan National Laboratory (Yerevan Physics Institute), Armenia

(Received 14 June 2011; revised manuscript received 23 January 2012; published 16 April 2012)

The basis of our analysis is the observation of the simultaneous enhancements of the gamma ray and neutron fluxes detected in 2009–2010 during thunderstorm ground enhancements at the mountain altitude of 3200 m. We investigate the correlated time series of the gamma rays and neutrons measured by the surface particle detectors of Aragats Space Environmental Center. The photonuclear reactions of the gamma rays born in the runaway breakdown (RB, now referred to as relativistic runaway electron avalanche, RREA) process with air were considered as the main process responsible for the copious neutron production. We consider also the mesoatom nuclei decay as a possible source of the additional neutrons registered by the neutron monitor due to enhanced population of the negative muons accelerated in the thunderclouds.

DOI: [10.1103/PhysRevD.85.085017](https://doi.org/10.1103/PhysRevD.85.085017)

PACS numbers: 92.60.Pw, 13.40.-f, 94.05.Dd

I. INTRODUCTION

The idea of neutron production during thunderstorms comes from the experimentation with fibers exploded after applying high voltage pulses. Neutron production in high voltage discharges forcing the explosion of fibers containing hydrogen or deuterium is reported in several papers (see [1], and references therein). An average neutron yield approached $\sim 10^{10}$ and neutron energy spectra peaked at 2.48 MeV. Based on these investigations, it was postulated that natural lightning discharges could produce neutrons as a mixture of deuterium contained in the atmospheric water vapor. However, the attempt to measure these neutrons in correlation with lightning strokes gives fluxes consistent with the cosmic ray background [2].

The first evidence of neutron generation in lightning discharges comes from Gulmarg, India, altitude 2743 m [3]. Neutrons were detected by the low-energy lead-free neutron monitor (GNM) comprising 21 proportional counters filled with BF_3 gas enriched by the B^{10} isotope ($\sim 3\%$ registration efficiency for 2.5 MeV neutrons). The counters were arranged in the form of a pile and were placed over 28 cm thick paraffin wax slabs 8 m above the ground. The counters were also covered by 7.5 cm thick paraffin wax. During the 3-year operation of the detector several lightning correlated neutron events were detected, the biggest one comprising 60 neutrons. The authors suggest a nuclear fusion [deuterium-deuterium, ($^2\text{H}, n$) ^3He] mechanism for producing 2.45 MeV neutrons occurring in the lightning channel. The neutron counting timing accuracy ($> 300 \mu\text{sec}$) was large compared to the duration of a lightning stroke, though, and there was no possibility to establish a one-to-one relation between lightning and detected neutrons.

Another Indian group running a neutron detection system at Mumbai (sea level) by statistical analysis

also claims correlation of neutron bursts with lightning [4]. The experimental device consisted of 16BF3 detectors of 0.05 m diameter, embedded in polyethylene neutron slowing-down material. The neutron burst was identified by the multiplicity greater than 2 (more than 2 neutrons detected by the system of 16 tubes within ~ 1 millisecond). During the low-altitude lightning occurrences the frequency of counts was significantly higher and multiplicities of 6 and 7 were observed (which were not observed during other weather conditions, including rain). The counts obtained during lightning were 4.8σ higher than the background. Therefore, the authors stated that neutron bursts were associated with lightning.

Recently the data acquisition electronics of the GNM has been significantly modified to record the time profiles of the neutron bursts with microsecond accuracy [5]. Despite a rather small amount of detected neutrons (the biggest event comprises 63 neutrons) and large millisecond delays of neutrons relative to lightning, the authors confirm the previous GNM claim of the production of neutrons in atmospheric discharges.

In the city of Sao Jose dos Campos, Brazil, at sea level a standard lead- and moderator-free He^3 tube (area 70 cm^2 ; type 25291; Ludlum, USA) detected a burst of neutrons which coincided with a lightning strike within a short distance of the detector (< 0.5 km). The minute count of 690 (the mean minute count rate was ~ 0.8) corresponds to the flux ~ 20 neutrons/ cm^2 , which in turn corresponds to about 10^{12} – 10^{13} neutrons produced by the lightning discharge [6].

A less exotic neutron source is associated with the excitation by gamma rays of natural oscillations of protons relative to neutrons, the so-called giant dipole resonance. When the gamma ray energy exceeds the energy of a giant resonance (the binding energy of the nucleon in the nucleus), neutrons that absorb the gamma rays escape from the nucleus [7].

*chili@aragats.am

Whether neutrons observed in correlation with lightning are produced by nuclear fusion or by photonuclear reaction remains uncertain. According to [8], though, the maximum bulk plasma temperature attained in lightning discharge is far too low to initiate fusion reactions. Photonuclear reactions in the air initiated by the gamma rays generated in the relativistic breakdown (RB, [9]), now referred as runaway electron avalanches (RREAs, [10]) seem to be a more probable process. Nonetheless, authors of Ref. [5] claim that there are some hot spots in the lightning channel where the pinch effect could create plasma configurations in which ions may have competing peak energies to induce fusion reactions.

Therefore, the problem of the neutron origin still is challenging. We need simultaneous detection of the gamma rays, neutrons, and lightning occurrence to disentangle this complicated problem. During last year's campaign at Aragats Space Environmental Center (ASEC, 2003, 2005) numerous thunderstorm ground enhancements (TGEs) were detected; some of them also include significant enhancements of the count rate of the Aragats Neutron Monitor (ANM). In this paper we present analysis of the simultaneous gamma ray and neutron enhancements and discuss possible explanations of the peaks in the ANM time series coinciding in time with gamma ray intensity increases.

A. Neutron enhancements detected by Aragats Neutron Monitor during thunderstorm ground enhancements

Registration of high-energy neutrons at ASEC was performed with the standard neutron supermonitor (NM-64, [11]), located at the slopes of Mt. Aragats near a lake at altitude of 3200 m. The neutron monitor registers basically the atmospheric neutrons in a wide range of energies, although with various efficiency, going down at low energies [12]. Eighteen cylindrical proportional counters of type CHM-15 (length 200 cm, diameter 15 cm) are filled with BF_3 gas enriched by a B^{10} isotope. The proportional chambers are surrounded by 5 cm of lead (producer) and 2 cm of polyethylene (moderator). The neutron supermonitor consists of 3 sections, 6 chambers in each. The cross section of lead producer above each section has a surface of $\sim 6 \text{ m}^2$, and a total surface of 3 sections— 18 m^2 . The atmospheric hadrons produce secondary neutrons in nuclear interactions in lead; then the neutrons get thermalized in a moderator, enter the sensitive volume of the counter, and in interactions with boron gas bear L_i^7 and the α particle. The α particle accelerates in the high electrical field inside the chamber and gives a pulse registered by the data acquisition electronics. The NM response to incident hadrons can contain several pulses depending on the number of secondary low-energy neutrons entering the volume of the counter and reacting with boron gas. Usually high-energy hadrons generate a larger number of secondary neutrons and have greater chances to generate more than

one pulse. If we want to count all pulses initiated by the incident hadron (i.e., estimate so-called multiplicities) we have to keep the dead time of the NM very low (the ANM has a minimal dead time of $0.4 \mu\text{s}$); if we want to count incident hadrons only (a one-to-one relation between count rate and hadron flux) we have to keep the dead time as much as all secondary neutron collecting time to avoid double counting (for ANM— $1250 \mu\text{s}$.)

For the detection of the thermal atmospheric neutrons on top of the ANM we install two proportional chambers without moderator and producer, only “bare” proportional counters. The 1 min time series of two chambers as well as 18 chambers of ANM are being entered in the MSQ database at CRD headquarters in Yerevan (available online from <http://adei.crd.yerphi.am/adei/>), and the database of the Euro-Asian consortium of neutron monitors (NMDB@.eu.org).

Other particle detectors of the ASEC [13,14] are continuously registering charged and neutral species of the secondary cosmic rays. The main building blocks of the particle detectors are plastic scintillators (both polished and molded pressed) located in the lightproof housings; the scintillation light is collected directly or via fiberglass light-shifting wires and overviewed by the photomultipliers. From the standard scintillation pieces of 5 cm thickness were assembled scintillator slabs from 20 to 60 cm thickness. The thin scintillators have very high efficiency to detect charged particles (mostly electrons and muons); the thick ones to detect neutral particles (gamma rays and neutrons). Thick detectors register also the energy deposit of traversing particles, thus giving the possibility to recover the energy spectra of the gamma ray flux. The coincidence technique allows significantly suppressing charged particle contamination to counts of thick scintillators and significantly purifying detected gamma ray flux. We use a 01 combination of the Aragats Solar Neutron Telescope (ASNT, 01 combination means no signal in the upper 5 cm thick scintillator and a signal in the 60 cm thick bottom scintillator) and 010 combination of the SEVAN¹ three-layered detector (signal only in the middle 20 cm thick scintillator). Details on detector operation can be found in [16].

In contrast to thick plastic scintillators, sensitive to both neutrons and gamma rays, the neutron monitor is sensitive only to incident hadrons (registration efficiency of electrons and gamma rays is negligible). The relative standard error of the particle detector 1 min time series is rather small (see Table I), ranging from 0.56% to 2%; therefore few percent peaks are significant and if the neutron peaks are correlated with electron and gamma ray peaks the chance probability of random coincidences is vanishingly

¹SEVAN is the worldwide network of hybrid particle detectors measuring neutral and charged components of the secondary cosmic rays, primarily aimed at space weather research and forecasting (see [15]).

TABLE I. Characteristics of ASEC particle detectors and parameters of the 4 October 2010 TGE.

Detector	Mean count rate per minute	Standard deviation (σ) and relative standard deviation	Percent of enhancement at 18:23, 4 October 2010	Number of standard deviations in peak at 18:23, 4 October 2010
SEVAN 010	2040	45 (2%)	73%	66σ
ASNT 01	31750	178 (0.56%)	32%	57σ
ANM	37700	285 (0.76%)	5.8%	7.6σ

small. We are also monitoring possible interferences and radio induced fake peaks and cleanup data from the suspicious channels.

The neutron event selection criteria consist of detection of the significant peaks in the neutron monitor 1 min time series coinciding in time with large peaks in gamma ray and electron fluxes measured by other ASEC particle detectors. An example of such an event is posted in Fig. 1.

At 18:23, 4 October 2010, all ASEC particle detectors registered large enhancements; see Fig. 1 and Table I.

Aragats neutron monitors were well maintained and corrected to atmospheric pressure changes and electronics aging [17]. In 2009–2010 when there were no interferences with peaks due to solar modulation effects (ground level enhancements and geomagnetic storms), we detected 12 peak enhancements of the neutron count rate observed by the ANM in coincidence with the enhanced gamma ray flux measured by other ASEC detectors; see Table II.

The first column of Table II provides the date of the TGE event.

In the second column we display the number of additional neutrons in the peak normalized to 1 m^2 .

In the third column we display the relative enhancement of neutrons in percent of the mean background, estimated by 1 h data before the start of the TGE,² and in the number of standard deviations.

In the fourth column we provide the neutron intensity at 3200 m obtained by the NM counts using the shape of the energy spectrum of the photonuclear neutrons and energy dependence of NM efficiency. The simulations were made by GEANT4 code; the primary gamma ray source was located at a height of 5000 m. The obtained neutron energy spectrum (see Fig. 2) coincided well with the spectrum presented in [18], Fig. 1. The energy dependence of the neutron monitor efficiency was taken according to Refs. [19–21].

In the fifth column we put the number of additional gamma rays in the peak detected by the ASNT. Also, we put in the fifth column the values of the reconstructed integral energy spectrum of gamma rays above 10 MeV. Only the two largest TGE events allow reliable gamma ray spectra recovering; for the rest of the events the histograms

of energy deposits in the 60 cm thick plastic scintillates of the ASNT detector (see details in [16]) are too scarce to allow reliable retrieving of the gamma ray energy spectra.

In the sixth column we put the relative enhancement of gamma rays in percent of the mean background and in number of standard deviations.

In the seventh column we put the recovered intensities of gamma rays for the 2 largest TGE events.

In the column 8 we put the ratio of neutron-to-gamma rays (for the largest two events also, the ratio of neutron-to-gamma ray intensities), which reveals some important features of neutron and gamma ray propagation in the atmosphere. As we see in column 8 for the 2 largest events the ratio of detected neutrons to detected gamma rays is substantially smaller compared with 10 other events. Thus, TGE events by gamma ray content fall in two groups: events detected on 19 September 2009 and 4 October 2010 and 10 other events.

In Fig. 3 we put the scatter plot of detected additional neutrons (x axis, from column 2 of Table II) vs number of additional gamma rays (y axis, from column 5 of Table II). In the scatter plot the existence of 2 distinct groups introduced above is apparent.

The existence of 2 distinct groups in the TGE events with different gamma ray content suggests that the parent gamma rays generated by the bremsstrahlung of the electrons accelerated in the RREA process have rather narrow lateral distribution. Only TGEs initiated by the RREA

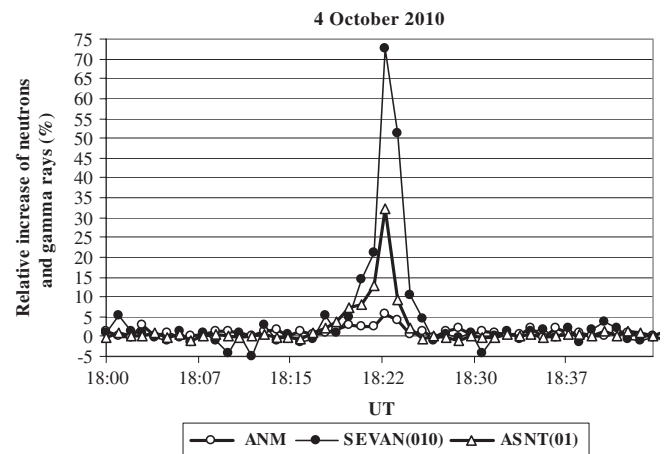


FIG. 1. The count rates of the ANM, SEVAN, and ASNT (01) combination on 4 October 2010.

²See for instance the mean count rate, standard deviation, and relative standard deviation of the background on 4 October 2010 in Table I.

TABLE II. The list of the parameters of the 12 TGE events with neutron content (2009–2010).

Day/month/year	Number of additional neutrons detected by ANM at minute of maximal excess (min ⁻¹ , m ⁻²)	Relative increase of neutrons detected by ANM (%)/N(σ)	Recovered neutron intensity at 3200 m (min ⁻¹ , m ⁻²)	Number of additional gamma rays detected by ASNT (combination 01) at minute of maximal excess min ⁻¹ , m ⁻²	Relative increase of gamma rays in (%)/N(σ)	Recovered gamma ray intensity at 3200 by (min ⁻¹ , m ⁻²)	Ratio of neutron to gamma ray flux/ ratio of intensities for largest TGE events
21/05/09 ^a	83	3.8/5	3420	1920	7/12		0.043
21/05/09 ^a	94	4.3/5.7	3847	1921	7/12		0.049
03/06/09 ^a	88	3.9/5.2	3613	1215	4/7		0.072
03/06/09 ^a	89	3.9/5.2	3666	1076	3.6/6		0.083
08/07/09 ^a	63	2.7/3.5	2591	1116	3.3/5.3		0.056
08/07/09 ^a	64	2.7/3.6	2624	1290	4.1/6.5		0.050
09/07/09	74	3.2/4.2	3050	1690	5.3/9.5		0.044
20/08/09	51	2.3/3.2	2110	940	3/4.8		0.054
02/09/09	50	2.5/3.3	2032	900	3/5.2		0.055
19/09/09	63	2.8/3.7	2574	7452	23/41	104 000	0.008/0.025
02/11/09	50	2.3/3.1	2041	1101	3.3/6		0.045
04/10/10	124	5.8/7.7	5091	10280	32/58	153 000	0.012/0.033

^aEvents occurred during 1 d but different times.

process above the particle detectors can sustain large gamma ray fluxes. The majority of the TGE events originate due to either modification of the energy spectra of cosmic ray electrons or the RREA process being launched outside the detector location site; in both cases the number of detected gamma rays will be significantly less.

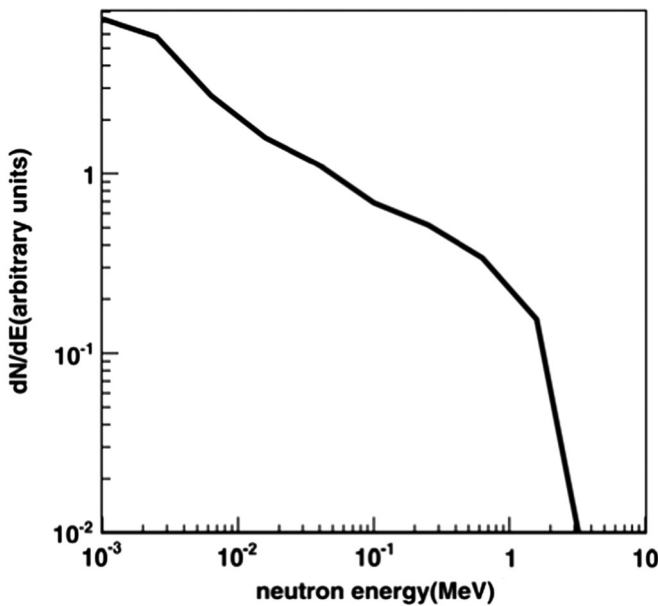


FIG. 2. Energy spectrum of neutrons born in photonuclear reaction; gamma ray source is located at 5000 m, and neutron detectors at 3200 m.

B. Contribution of the negative muons to ANM counts

The shift of the energy spectrum of the electrons/positrons and negative/positive muons entering a large electrical field region in thunderclouds can lead to dips and peaks in the time series of the count rates of surface particle detectors (see the theory of meteorological effects in [22] and numerical calculations in [23]). The charge ratio of positive-to-negative muons above 200 MeV equals ~1.3 [24,25]. Therefore, if an electrical field in the thundercloud is positive and accelerates electrons and negative muons downward, the same field will also decelerate positive muons. And, due to significant enhancement of the

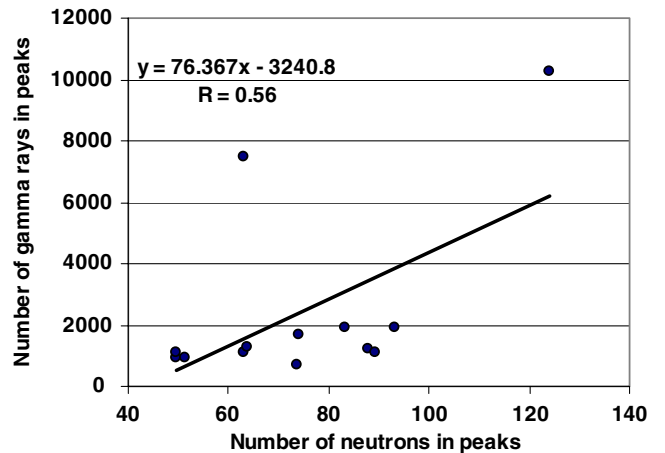


FIG. 3 (color online). Scatter plot of 12 TGE events detected in 2009–2010. *R* is correlation coefficient.

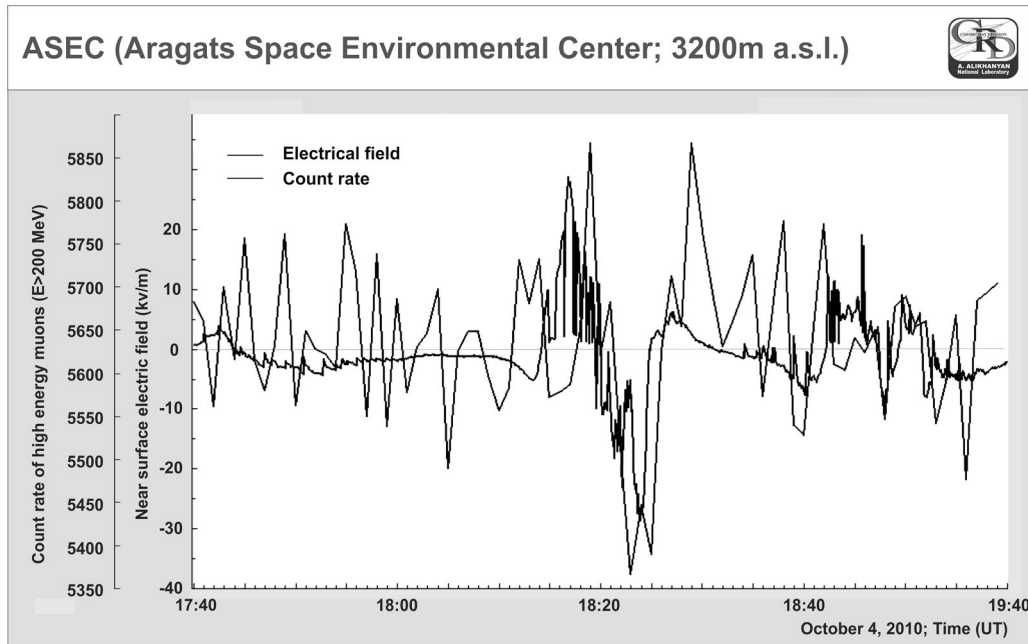


FIG. 4. Deficit of the >200 MeV muons during large negative near surface electrical field.

positive muons compared with the negative ones, we expect a dip in the time series of the high-energy muons at the same time when we detect enhancements of electrons and gamma rays. A SEVAN detector cannot distinguish between negative and positive muons—both charged particles are contributed to the time series registered by the detector—therefore, the detector count rate (the sum of negative and positive muons) after crossing the electrical field diminished because in the cosmic ray flux positive muons are 1.3 times more abundant than negative muons.

On 4 October we detected a deficit of the high-energy muons registered by SEVAN detectors' 111 combination (signals in each of the 3 layers of the assembly of 3 stacked scintillators interlayered by 10 cm of lead); see Fig. 4. As we can see in Fig. 4 the dip in the time series of high-energy muons coincides with a large negative field measured by an electrical mill located on the roof of the building where particle detectors are located.³ At the same time, with the same detector (see Fig. 1) we detect a huge enhancement of the gamma ray flux (a combination 010 of SEVAN).

The detected dip in the high-energy muon count rate indicates that the positive field in the thundercloud stopped the positive muons. Because the number of positive muons in the secondary cosmic rays' flux is ~ 1.3 times more compared with negative muons, we detect overall depletion of the muon flux (see Fig. 4). From the measured dip of $\sim 6\%$ in muon flux we calculate an expected deficit of the positive muons and enhancement of the negative muons. GEANT4 calculations indicate that the enhancement of the

negative muons can reach $\sim 15\%$ (consequently the reduction of positive muons is 20%). Consequently, the additional negative muons' incident on the ANM can be captured in the 5 cm thick lead producers of the ANM and form so-called mesic atoms where an electron orbiting the atom nucleus is substituted by the muon. Deexcitation of the nucleus occurs with emission of several MeV energy neutrons [22]. The details of nuclear muon capture and consequent decay with emission of several neutrons can be found in the review [26]. Therefore, several fractions of the neutron count rate enhancement can be attributed to these negative muons.

In Fig. 5 we depict the energy dependence of the efficiency of a negative muon to generate NM counts [27]. The efficiency of neutron detection is significant only in the energy range of 50–230 MeV. However, as demonstrated by our simulations the enhancement of the number of negative muons in this energy range after crossing the

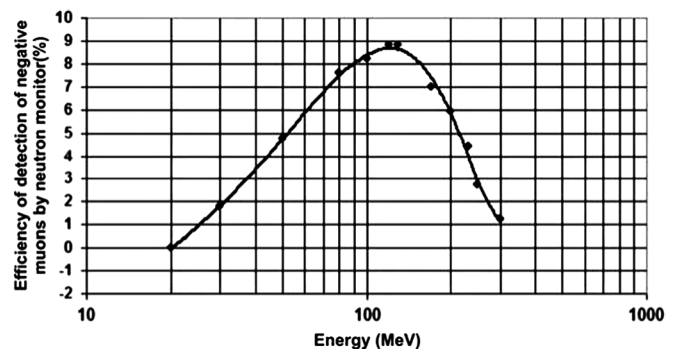


FIG. 5. Energy dependence of the NM detection efficiency of the negative muons.

³Almost all TGEs are detected during an abrupt decrease of the near surface electrical field down to ~ -30 kV/m.

electrical field is not very large. Therefore, from this calculation we cannot expect any significant (greater than 10–20) excess of NM count rate due to enhancement of the negative muons.

Another estimate of the additional count rate due to an enhanced number of negative muons [Eq. (30) from [22]] gives ~20 additional counts of the ANM. A simpler way to calculate additional NM counts is based on the estimate that 5%–7% of the overall NM counts is due to negative muons [28]. Let us assume that 6% of the NM count rate is generated by the negative muons; taking from Table I the ANM count rate (all 18 proportional tubes, ~1 m² surface each) we will obtain $37\,700 \times 0.06 = 2262$ additional counts from ambient population of secondary negative muons. On 4 October we estimated maximally ~15% of additional negative muons; therefore we can expect an additional $2262 \times 0.15 = 340$ NM counts; normalizing the additional flux to 1 m² we get ~20 additional counts among 124 detected on 4 October 2010.

C. Evidence of the “bare” proportional chamber

The bare (without lead producer and polyethylene moderator) proportional counter CNM-15, of the same type as is used in the ANM, was located directly above the ANM for detection of the low-energy neutrons. The bare counter registered enhancement on 4 October 2010 was well correlated with the ANM peak (see Fig. 6).

The number of neutrons detected during the 4 October 2010 TGE normalized to 1 m² was less than that of the ANM (54 and 124 correspondingly). Our simulations demonstrate that the MeV neutron flux incident on the neutron monitor thermalized in the polyethylene moderator and a significant fraction of the thermal neutrons is emitted upwards from the polyethylene moderator covering the ANM

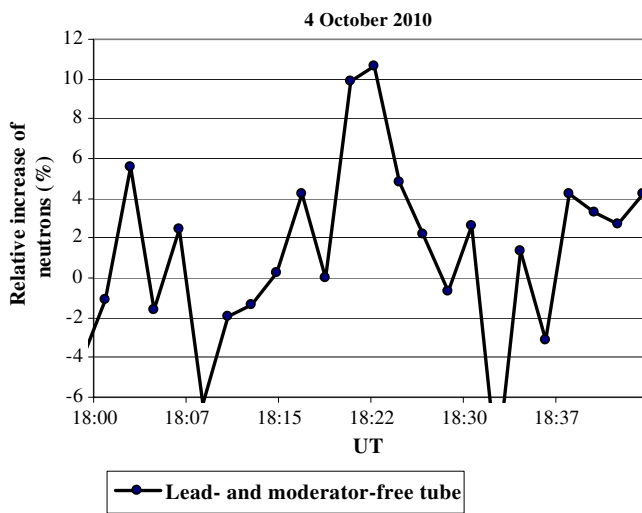


FIG. 6 (color online). Time series of the neutrons detected by bare proportional counter, located just on the ANM, 4 October 2010.

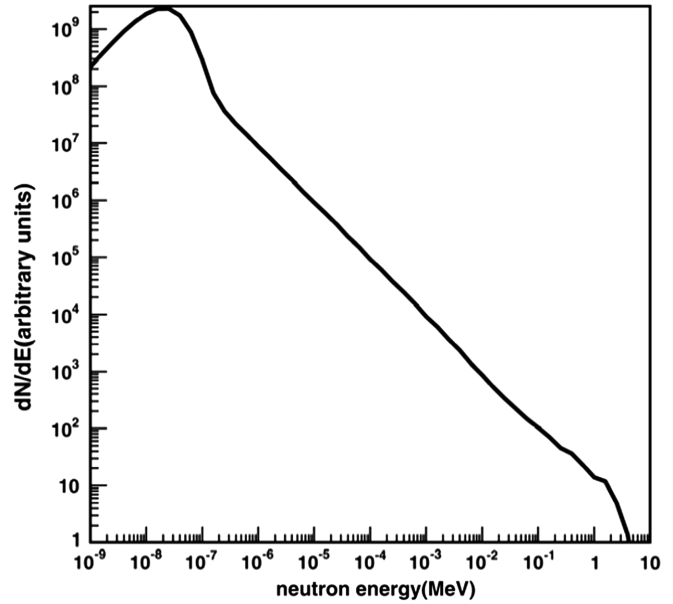


FIG. 7. Energy spectrum of the neutrons emitting upward from the polyethylene top layer of the ANM (logarithmic energy scale).

(the energy spectrum of the thermalized neutrons is depicted in Fig. 7).

The bare counter registered these neutrons having energies in the range (0.025–0.1 eV) with high efficiency [29]. Proceeding from the photonuclear neutron energy spectrum (Fig. 2) and the upward thermal neutron spectrum (Fig. 7), we simulate the expected number of hits in the bare counter on 4 October 2010 and come to an estimate of the neutron flux comparable with one we obtain by the NM counts.

II. DISCUSSION

Simultaneous detection of the electrons, gamma rays, and neutrons by experimental facilities of the Aragats Space Environmental Center provides a convincing confirmation of the photonuclear mechanism for neutron production during thunderstorms. The “lightning” origin of the neutrons can be ruled out because not all TGEs were accompanied by lightning occurrences⁴ and because the time scale of the neutron peaks in TGEs (minutes) drastically differs from the lightning time scale (milliseconds). The origin of the TGE is an extended region within a thundercloud between a negative charged layer and a positive charged layer in the bottom of the cloud (see Fig. 10 in [30]). Despite big varieties of electrical field profiles measured in the thundercloud the following basic structure of the electrical field in thunderclouds is widely accepted: from the ground up to the cloud base there is usually a low

⁴During the largest by neutron content 4 October 2010 TGE, with the neutron enhancement lasting ~5 minutes, we detected only one intracloud lightning occurrence.

magnitude field (both positive and negative); a relatively small positively charged “pocket” is lowermost just in the cloud base (comprising only $\sim 20\%$ of the negative charge higher up); a larger positive field prolongs up to a negative charge layer at 1–2 km above the cloud base; and the main positive charge is located about 1–4 km above the negative layer [31]. The lower positive charge region with the main negative layer in the middle of the cloud form, the so-called lower dipole, is responsible for the downward electron acceleration and also plays a major role in initiation of cloud-to-ground and intracloud lightning occurrences. Many researchers outline the dominant role the lower positive charge region plays in initiating/triggering intracloud and cloud-to-ground lightning discharges [32–34]. We suggest that development of the lower positive charge region also has a major role in TGE initiation.

The locality of the RREA can be explained by the small sizes of the lower positive charge region. Based on the detection of the winter thunderstorms in Japan, the authors of [35] estimate the radii of the circle of intense RREA radiation to be 600 m. Another Japanese group [36] detected movement at the speed of 7 m/sec of an energetic radiation source at the height of 300 m along with the negatively charged region within a thundercloud at the height of around 1 km. The radiation was emitted from a downward hemispherical surface with radii of 700 m. These findings demonstrate the locality of the RREA process and imply that the number of additional gamma rays can vary significantly depending on the “impact parameter” of the thundercloud relative to detection site (see also [37]). Therefore, a large discrepancy of the gamma ray content can be explained by the existence of 2 types of TGE events: one with a thundercloud above the detector location, and the second outside the detector location.

Gamma rays within the RREAs are radiated in a rather narrow cone; therefore they are illuminated in a limited area below the thundercloud. Only if RREAs occurred occasionally just above the site where particle detectors are located can we expect large fluxes of the RREA electrons and gamma rays like we detected during the 19 September 2009 and 4 October 2010 TGEs. The location of the majority of TGE events is outside the detector location site and detectors measure scattered gamma ray flux; the flux enhancement usually is rather small; the amplitude of 99% of TGEs is less than 10% of the cosmic ray background. Neutrons born in the photonuclear reactions have a much wider lateral distribution and can hit a neutron monitor even if the RREA is far from the detector site. And we can expect that the ratio of neutron-to-gamma ray content of the TGE will rise proportionally to the distance of the detector from the projection of the “center” of the lower dipole on the Earth’s surface.

To prove this statement we simulate RREA development and register gamma rays and neutrons in the circles of growing radii around the symmetry axes of the electron-

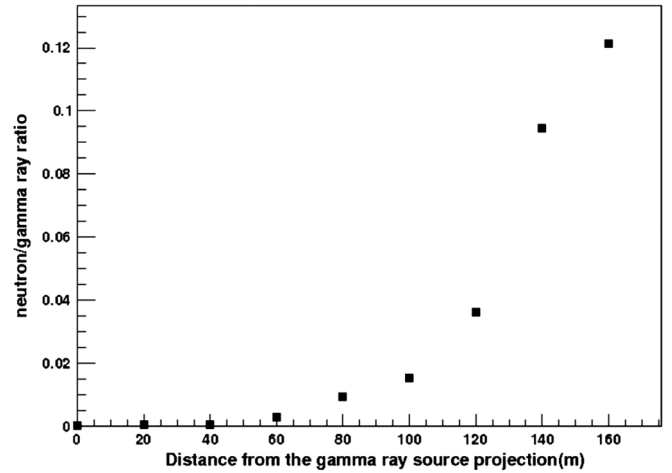


FIG. 8. Dependence of the detected-in-TGE neutron/gamma ray ratio on the distance from RREA center.

gamma ray avalanche. We again put the gamma ray source at 5000 m above the detector site located at 3200 m. The number of neutrons and gamma rays was counted in concentric rings of radii enlarging on each step by 20 m. As we can see from Fig. 8 the gamma content at distances less than 100 m is prevailing and the ratio is below 2%; however, at distances above 100 m the neutron-to-gamma ray ratio starts to rise very quickly reaching 12% at 160 m. As we can see in the last column of Table II the neutron-to-gamma ray ratio reconstructed for the 2 largest events is 2.5% and 3.3%; for the rest of the events, although we cannot recover intensities of the particle flux, proceeding from the measured count rate ratio we can expect a much larger value of neutron-to-gamma ray intensities. Of course, we recognize that the TGE is due to multiple RREA processes started from numerous points in an extended region in the thundercloud; however, as we discuss above, this region is local and the edge effect will lead to dependence of the neutron-to-gamma ray ratio similar to the one we display in Fig. 8.

III. CONCLUSIONS

We unambiguously prove the existence of the neutron flux linked to the TGEs and well correlated with the gamma ray flux. The mechanism of the neutron generation in the thunderclouds is the photonuclear reaction of the gamma rays born in the electron–gamma ray avalanches unleashed in the strong electrical fields of the thunderclouds (the RREA process).

Detection of the dips in the time series of the high-energy muons simultaneously with detection of very large peaks in low-energy gamma rays proves the existence of a large positive electrical field in the thunderclouds that accelerates electrons downward and demonstrates the developed positively charged layer in the bottom of the thundercloud.

ACKNOWLEDGMENTS

This work was partly supported by Armenian government grants and by Grant No. A1554 ISTC. The authors are grateful to participants of the conference TEPA-2010 and to members of the seminar of the cosmic ray division of the Yerevan Physics Institute for useful discussion and to

S. Chilingaryan for developing the ADEI multivariate visualization tool [38] for the treatment of the ASEC data flow. One of the authors (A. C.) is grateful to Brant Carlson for useful discussions on the start of work explaining the neutron content of TGE.

-
- [1] D. Klir *et al.*, *Phys. Plasmas* **15**, 032701 (2008).
 [2] R. L. Fleischer, *J. Geophys. Res.* **80**, 5005 (1975).
 [3] G. N. Shah, H. Razdan, C. L. Bhat, and Q. M. Ali, *Nature (London)* **313**, 773 (1985).
 [4] A. Shyam and T. C. Kaushik, *J. Geophys. Res.* **104**, 6867 (1999).
 [5] G. N. Shah, P. M. Ishtiaq, S. Mufti, and M. A. Darzi, in Burst Profile of the Lightning Generated Neutrons Detected by Gulmarg Neutron Monitor, 30th International Cosmic Ray Conference, Merida, Mexico, 2007.
 [6] I. M. Martin and M. A. Alves, *J. Geophys. Res.* **115**, A00E11 (2010).
 [7] J. Chadwick and M. Goldhaber, *Nature (London)* **134**, 237 (1934).
 [8] L. P. Babich and R. A. Roussel-Dupré, *J. Geophys. Res.* **112**, D13303 (2007).
 [9] A. V. Gurevich, G. M. Milikh, and Roussel-Dupre, *Phys. Lett. A* **165**, 463 (1992).
 [10] J. R. Dwyer, B. W. Grefenstette, and D. M. Smith, *Geophys. Res. Lett.* **35**, L02815 (2008).
 [11] H. Carmichael, “Cosmic Rays” (IQSY Instruction Manual, #7), London, 1964.
 [12] C. J. Hatton, in *Progress in Elementary Particles and Cosmic Ray Physics*, edited by J. G. Wilson and S. A. Wouthuysen (North Holland, Amsterdam, 1971), Vol. 10, p. 1.
 [13] A. Chilingarian *et al.*, *J. Phys. G* **29**, 939 (2003).
 [14] A. Chilingarian *et al.*, *Nucl. Instrum. Methods Phys. Res., Sect. A* **543**, 483 (2005).
 [15] A. Chilingarian and A. Reymers, *Ann. Geophys.* **26**, 249 (2008).
 [16] A. Chilingarian, A. Daryan, K. Arakelyan, A. Hovhannisyanyan, B. Mailyan, L. Melkumyan, G. Hovsepyan, S. Chilingaryan, A. Reymers, and L. Vanyan, *Phys. Rev. D* **82**, 043009 (2010).
 [17] A. Hovhannisyanyan and A. Chilingarian, *Adv. Space Res.* **47**, 1544 (2011).
 [18] B. E. Carlson, N. G. Lehtinen, and U. S. Inan, *J. Geophys. Res.* **115**, a00e19 (2010).
 [19] J. M. Clem and L. I. Dorman, *Space Sci. Rev.* **93**, 335 (2000).
 [20] E. A. Mauricev, B. B. Gvozdeckij, Yu. V. Balabin, and E. V. Vashenuk, Simulation of the Response Function of Neutron Monitors, official CD of Russian Cosmic Ray Conference, Moscow State Univ., 2010.
 [21] K. Watanabe *et al.*, *Astrophys. J.* **592**, 590 (2003).
 [22] L. I. Dorman and I. V. Dorman, *Adv. Space Res.* **35**, 476 (2005).
 [23] Y. Muraki *et al.*, *Phys. Rev. D* **69**, 123010 (2004).
 [24] J. Wentz, I. M. Brancus, A. Bercuci, D. Heck, J. Oehlschläger, H. Rebel, and B. Vulpescu, *Phys. Rev. D* **67**, 073020 (2003).
 [25] M. Bahmanabadi, F. Sheidaei, M. Khakian Ghomi, and J. Samimi, *Phys. Rev. D* **74**, 082006 (2006).
 [26] N. C. Mukhopadhyay, *Phys. Rep.* **30**, 1 (1977).
 [27] J. M. Clem, in *26th International Cosmic Ray Conference* (Salt Lake City, 1999), Vol. 7, p. 317.
 [28] E. B. Hughes and P. L. Marsden, *J. Geophys. Res.* **71**, 1435 (1966).
 [29] T. W. Crane and M. P. Baker, *Passive Nondestructive Assay of Nuclear Materials*, edited by D. Reilly *et al.* (Los Alamos National Laboratory, Los Alamos, NM, USA, 1991), Chap. 13, Technical Report No. NUREG/CR-5550, LA-UR-90-732.
 [30] A. Chilingarian, G. Hovsepyan, and A. Hovhannisyanyan, *Phys. Rev. D* **83**, 062001 (2011).
 [31] M. Stolzenburg, T. C. Marshall, and W. D. Rust, *J. Geophys. Res.* **103**, 14079 (1998).
 [32] A. Nag and V. A. Rakov, *Geophys. Res. Lett.* **36**, L05815 (2009).
 [33] S. D. Pawar and A. K. Kamra, *J. Geophys. Res.* **109**, D02205 (2004).
 [34] X. Qie, T. Zhang, C. Chen, G. Zhang, T. Zhang, and X. Kong, *Atmos. Res.* **91**, 244 (2009).
 [35] H. Tsuchiya *et al.*, *J. Geophys. Res.* **116**, D09113 (2011).
 [36] T. Torii, T. Sugita, M. Kamogawa, Y. Watanabe, and K. Kusunoki, *Geophys. Res. Lett.* **38**, L24801 (2011).
 [37] L. Babich, E. Bochkov, I. Kutsyk, and R. Roussel-Dupre, *J. Geophys. Res.* **115**, A00E28 (2010).
 [38] S. Chilingaryan, A. Beglarian, A. Kopmann, and S. Vöcking, *J. Phys. Conf. Ser.* **219**, 042034 (2010).